Journal of Materials Chemistry A

RSC Publishing

COMMUNICATION

View Article Online
View Journal | View Issue

Etched glass bubbles as robust micro-containers for self-healing materials†

Cite this: *J. Mater. Chem. A*, 2013, **1**, 12715

Received 15th August 2013
Accepted 3rd September 2013

DOI: 10.1039/c3ta13227g

www.rsc.org/MaterialsA

He Zhang and Jinglei Yang*

Etched glass bubbles (GBs) with through-holes at the micron level were fabricated by etching them using dilute hydrofluoric acid (HF) in a specially designed mixer. The semi-segmented mixer under mechanical agitation produces circulation of the GBs in solution, purposely completing the processes of the etching reaction on the GBs, filling the etched GBs with solution, and depositing the well etched GBs in the mixer bottom for collection. Highly reactive primary amine and diisocyanate monomer were separately infiltrated into the etched GBs and formulated as self-healing materials with satisfactory healing performance, indicating the robustness and versatility of the etched GBs.

The synthesis of mechanically robust, chemically and thermally stable micro-containers are the major challenges to develop instant, economical, and durable self-healing materials for practical engineering applications. After the first generation of self-healing material was realized by the incorporation of microcapsules containing dicyclopentadiene (DCPD) and the pre-dispersed Grubbs' catalyst,[1] quite a few self-healing systems have been developed,[2–8] among which the embedding of additive carriers containing reactive healing agent is a major approach for both structural composites and functional surface coatings due to its ease of manufacture and material integration.[9–22]

Currently, there is always a big challenge to apply highly reactive healing agents with ease of processing to realize instant repair of damage. As epoxy is a very important structural matrix, the homogeneous healing of it is very attractive to achieve better material compatibility and lower cost.[17,23–30] However, the most widely used hardeners, amines and their derivatives, have rarely been reported as healing agents due to their solubility in water and their reactivity. McIlory *et al.* demonstrated the breakthrough of direct encapsulation of a liquid amine derivative using a reverse emulsion method but did not provide sufficient self-healing data to assess these capsules's performance.[31] Jin *et al.* developed a two-step method to first synthesize polymeric hollow microcapsules and then infiltrate them with a modified aliphatic polyamine.[29] However, the long-term stability of the polymeric shell corroded by the amine degradation at elevated temperature limits their potential applications.[29] Isocyanate is another very promising healant as it can react with many chemicals that have active hydrogen atoms, including polyols, polyamines, polythiols, and even water or moisture in surroundings. Yang *et al.* for the first time reported the microencapsulation of a less reactive isophorone diisocyanate (IPDI) based on the interfacial polymerization of butanediol with toluene diisocyanate (TDI) prepolymer.[32] Recently, Huang and Yang demonstrated the microencapsulation of a more reactive hexamethylene diisocyanate (HDI) with the shell formed by the reaction of a polyol with a commercial prepolymer based on methylene diphenyl diisocyanate (MDI).[33] However, the susceptible water and solvent permeability and poor thermal stability of the microcapsule shell formed in the current microencapsulation methods highly restrict their engineering applications.[33]

It is highly desired to develop a method to produce mechanically robust, chemically and thermally stable micro-containers to store reactive agents for self-healing materials. An innovative method is herein proposed to address these issues by using modified GBs with small through-holes of micron size as universal healing agent carriers. Fig. 1 shows the whole procedure adopted in this study, which includes the etching of the GBs, the loading of the etched GBs with reactive chemicals, and the fabrication of self-healing samples with two-part and one-part healing mechanisms. The GBs were etched by diluted 1% HF solution using a specially designed device consisting of three parts, *i.e.* a mixer with three segmented but connected zones, a curved four-blade propeller, and a feeder with a tubule extension for the gradual addition of HF solution, as shown in

School of Mechanical and Aerospace Engineering, Nanyang Technological University, 50 Nanyang Avenue, 639798, Singapore. E-mail: mjlyang@ntu.edu.sg; Tel: +65 67906906

† Electronic supplementary information (ESI) available. See DOI: 10.1039/c3ta13227g

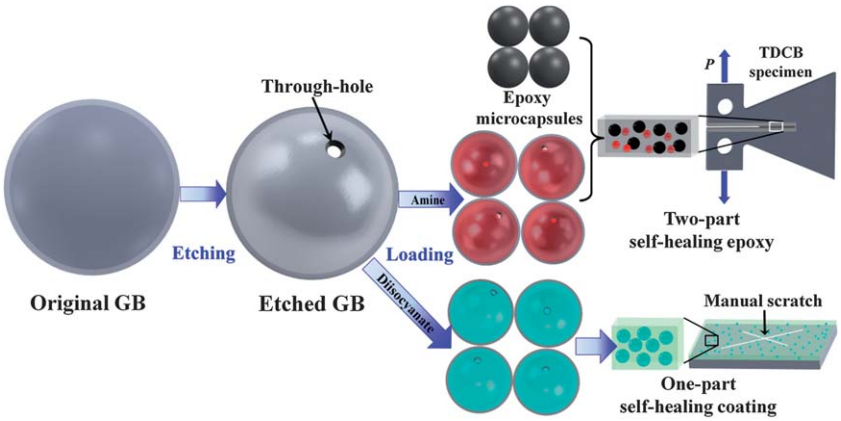

Fig. 1 The schematic illustration (not to scale) of the whole experimental process, including the etching of GBs, the loading of the etched GBs, and the sample preparation of two-part self-healing epoxy and one-part self-healing coating. The healing performances of self-healing epoxy and coating were characterized using the TDCB specimen (top right image) and the coated metal substrate (bottom right image), respectively.

Fig. 2a. The three semi-segmented zones with different functions from top to bottom are: the reaction zone with gentle agitation for the etching reaction and circulation of GBs; the separation zone for the separating and sinking of the well-etched GBs from the intact ones; and the collection zone for the deposition of the well-etched GBs. The separating and sinking function of the separation zone is attributed to the quasi-static feature originating from the inserted separation meshes and cross barriers. In order to impede the HF from the two top zones moving into the bottom collection zone to further etch the deposited GBs, a separator with a long tubule is inserted between the separation zone and the collection zone. The edge between the separator and the mixer is well sealed for better isolation. Fig. 2b shows the etching process by the manufactured practical reaction system in our lab. Every part of the system runs as designed. The enlargement in Fig. 2c illustrates the deposition of the GBs through the small tubule of the separator during etching.

The controllability of this system lies in the separation of the well-etched GBs from the intact ones, and the further deposition of them at the bottom simultaneously and continuously brought by the introduction of the three different zones in the same mixer. During etching, intact GBs with low density participate in circulation under mild stirring in the mixer. Once small holes form in the shell by etching, solution will infiltrate into the etched GBs therein gradually. With the increase of solution in the cavity of the etched GBs, their density increases and finally becomes larger than that of the solution. When these etched GBs circulate to the quasi-static separation zone, they will separate from the intact GBs automatically as shown in the

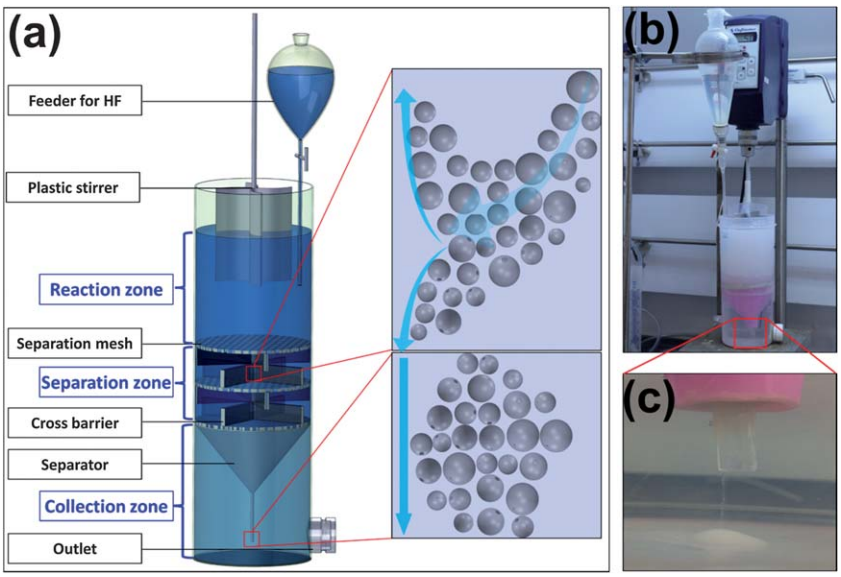

Fig. 2 (a) The schematic configuration of the specially designed etching system with interconnected segmented zones; (b) the real image of the reaction system during etching; (c) the enlarged tip in the collection zone showing the deposition of the well-etched GBs.

scheme at top right in Fig. 2a, and finally deposit onto the bottom through the tubule of the separator for collection, as illustrated by the scheme at bottom right in Fig. 2a and the enlargement in Fig. 2c. Consequently, the etched GBs with holes and thinner walls, which can be easily broken by the propeller and further etched by the HF solution, keep stationary in the collection zone rather than circulating and reacting in the top zones. The through-holes in the GBs will be prevented from over-etching if this mixer is employed.

Fig. 3a shows the SEM image of the as-received spherical GBs with diameters ranging from 63 μm to 90 μm and wall thickness of around 1 μm (inset image) after removing debris. The shell thickness measured from more than 50 different broken GBs is 1.16 μm with a large standard deviation of 0.57 μm, indicating that the thickness of the glass shell is not uniformly distributed. The enlarged SEM images reveal that all the GBs have smooth outer surface dotted with nanoparticles, as shown in Fig. 3b. In addition, some existing defective areas with loose structure and microcrack are observed in Fig. 3b and c, respectively. Both thinner regions due to uneven thickness and pre-defective areas of GBs with loose structure are prone to be etched to form through-holes.

The etched GBs after water-deposition to remove debris are shown in Fig. 3d. Additional overview image of the etched GBs can be found in Fig. S1.† Compared with the original bubbles, the etched ones show three major changes in their profiles. Firstly, the smooth outer surface with nanoparticles was etched to rough region with uniformly distributed nano-pits (Fig. 3e), which can be attributed to locally uneven reacting rate and might bring another benefit to enhance interfacial bonding strength when used in a polymeric matrix. Secondly, through-holes at the micron level were formed in the glass wall, as shown in Fig. 3e–g. The thin-edged through-holes presented in Fig. 3e and f may be etched from thinner walls or existing cracked areas as shown in Fig. 3c, while the sharp through-hole shown in Fig. 3g may be formed from the loose structure shown in Fig. 3b. Since the formation of a through-hole on the GB will lead to its deposition to avoid over-etching of the GB, very few holes could be formed in one bubble, which can be verified by the images of the etched GBs in Fig. 3d and Fig. S1.† Lastly, the shell thickness was reduced from 1.16 ± 0.57 μm to 0.79 ± 0.41 μm after the overall etching process, as typically shown as the inset image in Fig. 3d.

As an application of the etched GBs, a self-healing epoxy was prepared using two-part epoxy-amine chemistry by amine loaded GBs and epoxy filled microcapsules, as shown at the top right in Fig. 1. The amine solution was infiltrated into the etched GBs using the device as illustrated in Fig. S2,† and the epoxy solution was encapsulated by poly(ureaformaldehyde) (PUF) shell as shown in Fig. S3.† First the dispersion of the loaded GBs and epoxy filled microcapsules in the epoxy matrix were checked by optical microscopy, as shown in Fig. 4a after curing at room temperature (20 °C) for 4 h. It is revealed that almost all the GBs were fully loaded with amine solution, and that the two healing agent carriers were well dispersed in the epoxy matrix. Although there are small through-holes on every etched GB, the amine loaded in these GBs after their incorporation into the epoxy matrix shows relatively high stability during the curing process, which can be seen from the optical microscopic images of the mixture after being cured at room temperature for 24 h (Fig. S4a†) and then 35 °C for another 24 h

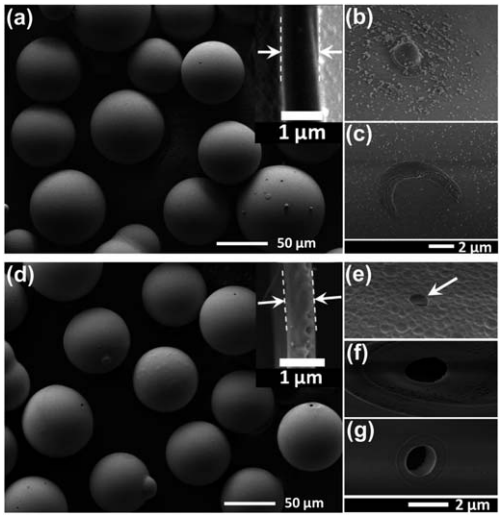

Fig. 3 (a) The overview of the original GBs in 63–90 μm after water deposition; (b) and (c) the defects in the shell; (d) the etched GBs in 63–90 μm after water deposition; (e)–(g) the through-holes etched in the shell. The insets in (a) and (d) show the cross-sectional thickness of the original and etched GB, respectively.

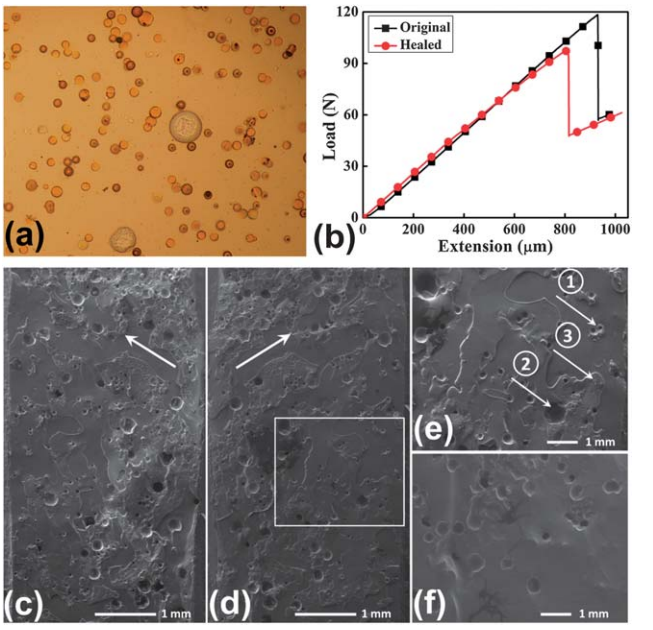

Fig. 4 (a) Optical microscopic images showing the dispersion of the loaded GBs (small spheres) embedded in the epoxy together with epoxy filled microcapsules (large spheres) after room temperature curing for 4 h; (b) the fracture load-displacement curves for a sample before and after healing using the TDCB specimen; (c) and (d) a mirrored region of the fracture surfaces after healing at 50 °C for 24 h; (e) the enlarged frame in (d) showing a fractured GB (arrow 1), a fractured microcapsule (arrow 2), and the newly formed thin film (arrow 3) by the released healing agents; (f) the fracture surface of the control specimen incorporated with epoxy filled microcapsules only.

(Fig. S4b†). Fig. S5a–f† show the thermal stability of the loaded amine in the etched GBs at room temperature for 1, 2, 4, 8, 16, and 32 days, respectively. It can be observed that after about 1 month (Fig. S5f†), almost all the loaded GBs are full with amine, just as the appearance when they were freshly incorporated (Fig. S5a†). Those observations demonstrate that the small holes at micron level in the etched GBs are so tightly sealed by the surrounding cured epoxy that the evaporation and diffusion of the amine is significantly retarded or even completely restricted.

The healing efficiency was characterized by the recovered percentage of mode I fracture toughness using short-grooved tapered double cantilever beam (TDCB) specimens, as illustrated in Fig. 1 at top right. The typical load-displacement curves of the specimen for the original fracture and healed fracture are given in Fig. 4b. After healing at 50 °C for 24 h,

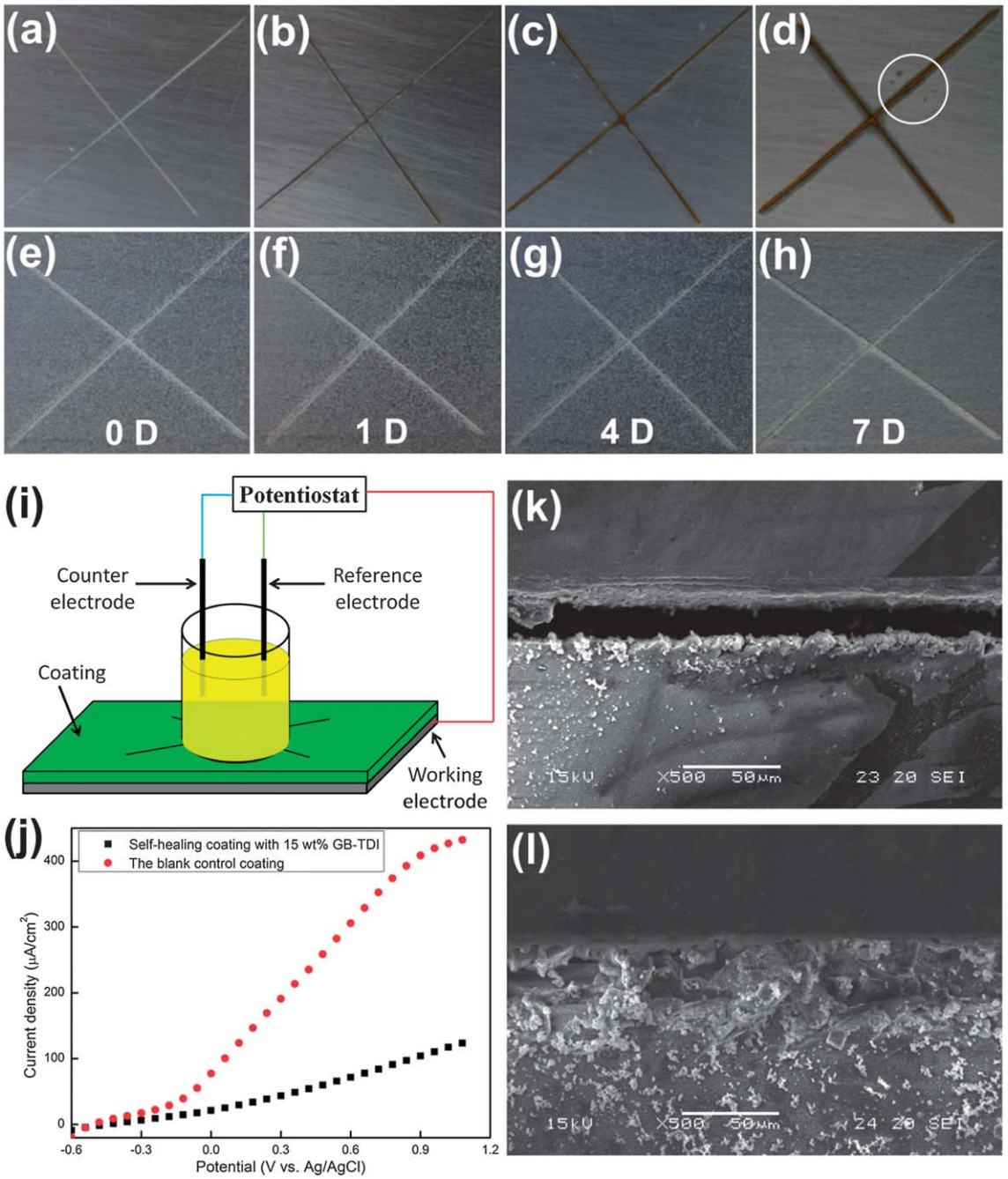

Fig. 5 The self-healing behavior of the coatings containing 15 wt% TDI loaded GBs. (a)–(d) The digital images for the corrosion performance of the control coating immediately after scratching (0 D) and after immersion in 1 M NaCl solution for 1, 4, and 7 days, the white circle in (d) indicates the etching pits; (e)–(h) the digital images for the corrosion performance of the self-healing coating right after scratching (0 D) and after immersion in 1 M NaCl solution for 1, 4, and 7 days; (i) the schematic setup for the electrochemical test; (j) the polarization resistance curves for the control and self-healing coating. The SEM images for the scratched area of the control coating (k) and the self-healing coating (l).

average healing efficiency of 93 ± 17.2% was obtained when 11.25 wt% amine loaded GBs and 3.75 wt% epoxy filled microcapsules were mixed into epoxy matrix in this study. This healing efficiency is quite close to the healing performance (91.1 ± 6.5%) at the same healing condition by injection of excess amount of epoxy mixture with stoichiometric amine hardener. For the control specimens with pure epoxy or epoxy incorporated with only epoxy filled microcapsules, no healing was found after the same healing condition.

A typical morphology of the mirrored fracture surface is shown in Fig. 4c and d. The arrow 1 and arrow 2 in Fig. 4e indicate a fractured GB and a fractured microcapsule, respectively. The epoxy thin film newly formed by the released healing agents is clearly observed at the fracture surface (arrow 3 in Fig. 4e). Compared with the smooth fracture surface of the control specimen incorporated with only epoxy filled microcapsules (Fig. 4f), this new film adhered the two fracture surfaces, recovering most of the load bearing ability. Compared with the adhesive failure of the healed epoxy realized in the DCPD-Grubbs' catalyst system,[1] the cohesive failure in this case demonstrates that the bonding strength of the interface is higher than the fracture strength of the formed epoxy film due to the homogeneous healing by the two-part epoxy-amine chemistry.

Another example to show the feasibility and versatility of the etched GBs is that they were loaded with very reactive diisocyanate, toluene diisocyanate (TDI), and mixed into UV curable resin, Norland Optical Adhesive (NOA) 61, to prepare self-healing anti-corrosive coating on steel substrates, as shown at bottom right in Fig. 1. Fig. 5a–h show the corrosion process of the scratched control and self-healing specimens right after scratching (0 day) and after immersion in the 1 M sodium chloride (NaCl) solution for 1, 4, and 7 days (more digital images given in Fig. S6†). Compared with the control specimen with rust growing gradually in the scratches after immersion in the corrosive solution, the self-healing coating stayed unchanged as in the original appearance. Besides that, the area corroded by the salt solution spread beneath the coating near the scratch for the control specimen.

After 7 days, no change was observed at the self-healing specimen while serious corrosion took place at the control specimen, resulting in the color of the scratch darker and the corroded area wider. And some etching pits, as indicated by the circle in Fig. 5d, appeared and grew around the seventh day. Fig. 5i and j separately give the schematic setup of the electrochemical test and the corresponding polarization resistance curves of the two coatings after immersion in salt solution for 7 days. Compared with the rapid increase of the current density accompanied with the increased potential for the control specimen, the change of the current density for the self-healing specimen is much smaller. This electrochemical behavior verifies the self-healing functionality introduced by TDI loaded GBs. The SEM images in Fig. 5k and l show the scratched area in the control and self-healing coatings, respectively. The scratch in the self-healing coating was well sealed by the released TDI from the ruptured GBs during scratching while the open scratch in the control coating was empty with nothing. As stated before by Huang and Yang,[33] the incorporated TDI loaded GBs can achieve self-healing and anti-corrosive functionalities in two aspects: the sealing of the scratch by the formed polyurea wedge from reaction of the released TDI with water in surroundings (Fig. 5j), and the depletion of the diffused water through the coating by the TDI in the intact GBs to avoid the pitting corrosion (circle in Fig. 5d).

In summary, we reported the fabrication of GBs with small through-holes which were controllably etched by dilute 1% HF solution using a specially designed reaction system. The GBs were etched as expected in the mixer to achieve the small through-holes in the shell. A self-healing epoxy and a self-healing anti-corrosive coating based on the etched GBs loaded with different healants were successfully fabricated to verify their self-healing performance in terms of the recovered mode I fracture toughness and scratch-sealing behavior, respectively. The highest healing efficiency for the self-healing epoxy of about 93% was obtained when the specimens were incorporated with 11.25 wt% amine loaded GBs and 3.75 wt% epoxy filled microcapsules and healed at 50 °C for 24 h after fracture. Cohesive failure of the crack plane was found during the fracture after healing. As for the self-healing anti-corrosive coating, almost complete sealing of the scratch was achieved and protection of the intact area from pitting corrosion was found by the incorporation of TDI loaded GBs.

Acknowledgements

Yang is grateful for the financial support of this work from the NTU Start-up grant and Singapore MoE Tier 1 research fund (Grant #: RG17/09).

References

1 S. R. White, N. R. Sottos, P. H. Geubelle, J. S. Moore, M. R. Kessler, S. R. Sriram, E. N. Brown and S. Viswanathan, *Nature*, 2001, **409**, 794–797.
2 D. Y. Wu, S. Meure and D. Solomon, *Prog. Polym. Sci.*, 2008, **33**, 479–522.
3 B. J. Blaiszik, S. L. B. Kramer, S. C. Olugebefola, J. S. Moore, N. R. Sottos and S. R. White, *Annu. Rev. Mater. Res.*, 2010, **40**, 179–211.
4 S. Burattini, B. W. Greenland, D. Chappell, H. M. Colquhoun and W. Hayes, *Chem. Soc. Rev.*, 2010, **39**, 1973–1985.
5 M. D. Hager, P. Greil, C. Leyens, S. van der Zwaag and U. S. Schubert, *Adv. Mater.*, 2010, **22**, 5424–5430.
6 E. B. Murphy and F. Wudl, *Prog. Polym. Sci.*, 2010, **35**, 223–251.
7 J. A. Syrett, C. R. Becer and D. M. Haddleton, *Polym. Chem.*, 2010, **1**, 978–987.
8 J. L. Yang, H. Zhang and M. X. Huang, *Emerging Technology in Aerospace Engineering: Polymer-Based Self-Healing Materials in Aerospace Materials Handbook*, CRC Press, 2012.
9 X. X. Chen, M. A. Dam, K. Ono, A. Mal, H. B. Shen, S. R. Nutt, K. Sheran and F. Wudl, *Science*, 2002, **295**, 1698–1702.
10 D. Therriault, S. R. White and J. A. Lewis, *Nat. Mater.*, 2003, **2**, 265–271.
11 D. Therriault, R. F. Shepherd, S. R. White and J. A. Lewis, *Adv. Mater.*, 2005, **17**, 395–399.

12 D. G. Shchukin, M. Zheludkevich, K. Yasakau, S. Lamaka, M. G. S. Ferreira and H. Möhwald, *Adv. Mater.*, 2006, **18**, 1672–1678.
13 K. S. Toohey, N. R. Sottos, J. A. Lewis, J. S. Moore and S. R. White, *Nat. Mater.*, 2007, **6**, 581–585.
14 N. W. Choi, M. Cabodi, B. Held, J. P. Gleghorn, L. J. Bonassar and A. D. Stroock, *Nat. Mater.*, 2007, **6**, 908–915.
15 M. W. Keller, S. R. White and N. R. Sottos, *Adv. Funct. Mater.*, 2007, **17**, 2399–2404.
16 P. Cordier, F. Tournilhac, C. Soulie-Ziakovic and L. Leibler, *Nature*, 2008, **451**, 977–980.
17 K. S. Toohey, C. J. Hansen, J. A. Lewis, S. R. White and N. R. Sottos, *Adv. Funct. Mater.*, 2009, **19**, 1399–1405.
18 B. Ghosh and M. W. Urban, *Science*, 2009, **323**, 1458–1460.
19 Q. Wang, J. L. Mynar, M. Yoshida, E. Lee, M. Lee, K. Okuro, K. Kinbara and T. Aida, *Nature*, 2010, **463**, 339–343.
20 A. C. Jackson, J. A. Bartelt and P. V. Braun, *Adv. Funct. Mater.*, 2011, **21**, 4705–4711.
21 M. Burnworth, L. M. Tang, J. R. Kumpfer, A. J. Duncan, F. L. Beyer, G. L. Fiore, S. J. Rowan and C. Weder, *Nature*, 2011, **472**, 334–337.
22 Y. Chen, A. M. Kushner, G. A. Williams and Z. Guan, *Nat. Chem.*, 2012, **4**, 467–472.
23 M. Motuku, U. K. Vaidya and G. M. Janowski, *Smart Mater. Struct.*, 1999, **8**, 623–638.
24 J. W. C. Pang and I. P. Bond, *Compos. Sci. Technol.*, 2005, **65**, 1791–1799.
25 G. Williams, R. Trask and I. Bond, *Composites, Part A*, 2007, **38**, 1525–1532.
26 M. M. Caruso, B. J. Blaiszik, S. R. White, N. R. Sottos and J. S. Moore, *Adv. Funct. Mater.*, 2008, **18**, 1898–1904.
27 Y. C. Yuan, M. Z. Rong, M. Q. Zhang, B. Chen, G. C. Yang and X. M. Li, *Macromolecules*, 2008, **41**, 5197–5202.
28 D. S. Xiao, Y. C. Yuan, M. Z. Rong and M. Q. Zhang, *Adv. Funct. Mater.*, 2009, **19**, 2289–2296.
29 H. Jin, C. L. Mangun, D. S. Stradley, J. S. Moore, N. R. Sottos and S. R. White, *Polymer*, 2012, **53**, 581–587.
30 S. H. Teoh, H. Y. Chia, M. S. Lee, A. J. N. Nasyitah, H. B. S. M. Luqman, S. Nurhidayah and W. C. K. Tan, *Int. J. Mod. Phys. B*, 2010, **24**, 157–163.
31 D. A. McIlroy, B. J. Blaiszik, M. M. Caruso, S. R. White, J. S. Moore and N. R. Sottos, *Macromolecules*, 2010, **43**, 1855–1859.
32 J. L. Yang, M. W. Keller, J. S. Moore, S. R. White and N. R. Sottos, *Macromolecules*, 2008, **41**, 9650–9655.
33 M. X. Huang and J. L. Yang, *J. Mater. Chem.*, 2011, **21**, 11123–11130.

